

# Clutter-Aware Target Detection for ISAC in a Millimeter-Wave Cell-Free Massive MIMO System

Steven Rivetti<sup>†</sup>, Özlem Tuğfe Demir\*, Emil Björnson<sup>†</sup>, Mikael Skoglund<sup>†</sup>

<sup>†</sup>School of Electrical Engineering and Computer Science (EECS), KTH Royal Institute of Technology, Sweden

\*Department of Electrical-Electronics Engineering, TOBB University of Economics and Technology, Ankara, Türkiye

**Abstract**—In this paper, we investigate the performance of an integrated sensing and communication (ISAC) system within a cell-free massive multiple-input multiple-output (MIMO) system. Each access point (AP) operates in the millimeter-wave (mmWave) frequency band. The APs jointly serve the user equipments (UEs) in the downlink while simultaneously detecting a target through dedicated sensing beams, which are directed toward a reconfigurable intelligent surface (RIS). Although the AP-RIS, RIS-target, and AP-target channels have both line-of-sight (LoS) and non-line-of-sight (NLoS) parts, it is assumed only knowledge of the LoS paths is available. A key contribution of this study is the consideration of clutter, which degrades the target detection if not handled. We propose an algorithm to alternatively optimize the transmit power allocation and the RIS phase-shift matrix, maximizing the target signal-to-clutter-plus-noise ratio (SCNR) while ensuring a minimum signal-to-interference-plus-noise ratio (SINR) for the UEs. Numerical results demonstrate that exploiting clutter subspace significantly enhances detection probability, particularly at high clutter-to-noise ratios, and reveal that an increased number of transmit side clusters impair detection performance. Finally, we highlight the performance gains achieved using a dedicated sensing stream.

**Index Terms**—RIS, ISAC, cell-free massive MIMO, mmWave.

## I. INTRODUCTION

Cell-free massive multiple-input multiple-output (MIMO) is a user-centric network infrastructure where a set of distributed access points (APs) serve multiple user equipments (UEs) on the same time-frequency resources using joint processing techniques [1]. Over nearly a decade of research, it has been shown that cell-free massive MIMO improves both spectral and energy efficiency by providing macro diversity and enhanced interference management compared to traditional cellular setups. As a result, it has become one of the key technologies for sixth-generation (6G) wireless networks [2].

Recently, the cell-free massive MIMO architecture has also demonstrated potential benefits in integrated sensing and communications (ISAC) [3], [4]. ISAC allows for the efficient use of hardware and spectral resources through integration and coordination gains, compared to separate communication and sensing architectures [5]. Cell-free massive MIMO facilitates multi-static sensing through a central processing unit (CPU), to which the APs are connected via fronthaul links. Beyond cell-free massive MIMO and ISAC, another key 6G

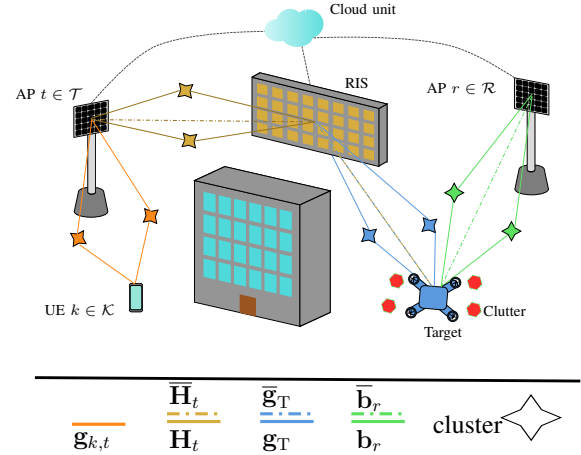


Fig. 1: Depiction of a cell-free massive MIMO ISAC network performing multi-static sensing.

technology is reconfigurable intelligent surface (RIS)-aided communications. RISs have attracted significant attention from both academia and industry due to their ability to control challenging radio propagation environments intelligently. By using low-cost passive reflecting elements that induce controllable phase shifts in incoming waveforms, RISs can steer reflected signals toward desired locations while reducing interference at undesired points [6], [7]. Furthermore, RISs have emerged as a promising technology in ISAC applications, enhancing the available spatial degrees-of-freedom. In [8], the sum rate of communication UEs is maximized under a worst-case sensing signal-to-noise ratio (SNR) constraint. An often overlooked aspect in ISAC research is the effect of clutter on target detection, which can severely degrade system performance if not properly addressed. Recent studies, such as [9], illustrate the impact of clutter in monostatic ISAC settings, underscoring the significance of clutter awareness at the receiving APs for reliable target detection.

In this paper, we investigate the extent to which an RIS can enhance sensing capabilities when the direct channels between the transmitting APs and the target are obstructed. We also explore the need for precise channel state information (CSI) for target detection within a millimeter-wave (mmWave) channel architecture, as well as the requirement for sensing-specific streams. Our setup, illustrated in Fig. 1, evaluates the system's ability to detect a potential target at a known location while meeting a minimum signal-to-interference-plus-

This work was supported by the SUCCESS project (FUS21-0026), funded by the Swedish Foundation for Strategic Research. Ö. T. Demir was supported by 2232-B International Fellowship for Early Stage Researchers Programme funded by the Scientific and Technological Research Council of Türkiye.

noise ratio (SINR) for each UE. To this extent, we maximize the target's signal-to-clutter-and-noise ratio (SCNR) using an alternating optimization (AO) algorithm that jointly optimizes transmit power allocation and the RIS phase-shift matrix. The APs assume a line-of-sight (LoS) structure for the sensing links, justified by the high path loss in mmWave frequencies, which typically makes LoS paths dominant over non-line-of-sight (NLoS) paths. A centralized precoding strategy is employed with regularized zero forcing (RZF) for communication streams. The sensing stream is projected onto the null space of the communication channels, which are assumed to be known at the APs. Assuming knowledge of the clutter subspace, target detection is conducted using a generalized likelihood ratio test (GLRT). The numerical simulations reveal that clutter awareness significantly enhances the detection probability, particularly at high clutter-to-noise ratio (CNR). Furthermore, when sensing links contain many clusters concentrated in a narrow angular range, the LoS assumption becomes less effective, reducing detection probability. The results also highlight the importance of allocating dedicated sensing symbols to improve detection performance.

*Notation:*  $\odot$  represents the Hadamard (element-wise) product. Boldface lowercase and uppercase letters denote vectors and matrices. The trace of the matrix  $\mathbf{X}$  is denoted by  $\text{Tr}(\mathbf{X})$ .  $\text{diag}(\mathbf{x})$  represents the stacking of  $\mathbf{x}$  on the main diagonal of a matrix.  $\mathbf{I}_N$  represents an  $N \times N$  identity matrix. The notation  $\mathcal{CN}(0, \sigma^2)$  represents circularly symmetric complex Gaussian distribution with variance  $\sigma^2$ . By  $\mathcal{L} \setminus \{l\}$ , we denote the set obtained by removing the element  $l$  from the set  $\mathcal{L}$ . Given a matrix  $\mathbf{M}$ ,  $\mathbf{M}^\dagger$  represents its Moore-Penrose pseudoinverse.

## II. SYSTEM MODEL

We consider the RIS-assisted cell-free massive MIMO ISAC network shown in Fig. 1. Here a set  $\mathcal{T}$ , whose cardinality is  $|\mathcal{T}| = T$ , of APs, each equipped with  $M$  transmit antennas, serves  $K$  single-antenna UEs in the downlink while sensing the potential presence of a target at a known position. The sensing is assumed to be carried out over  $U$  symbols belonging to the same channel coherence block. A second set of APs, denoted by  $\mathcal{R}$ , with  $|\mathcal{R}| = R$ , collects the echos backscattered from the target and performs target detection. The choice of geographically separated transmitting and receiving APs is motivated by the implementation challenges of full duplex operation, especially in terms of self interference [10], and the interest in this setup for cell-free massive MIMO communications. We assume that the direct channel between  $\mathcal{T}$  and the target is blocked and, thus, the former reaches the target through a RIS equipped with  $N$  reflective elements whose phase shifts are described by the vector  $\boldsymbol{\theta} = [\theta_1, \dots, \theta_N]^\top$ , where  $|\theta_n| = 1$  for  $n = 1, \dots, N$ . Each AP  $t \in \mathcal{T}$  is connected to the RIS via the channel  $\mathbf{H}_t \in \mathbb{C}^{N \times M}$ , the reflected path connecting the RIS to the target is denoted by  $\mathbf{g}_T \in \mathbb{C}^N$  and the UEs are connected to the APs in  $\mathcal{T}$  via the channel  $\{\mathbf{g}_{k,t}\}_{\forall k,t} \in \mathbb{C}^M$ . The receiving APs in  $\mathcal{R}$  are connected to the target via the channels  $\{\mathbf{b}_r\}_{\forall r \in \mathcal{R}} \in \mathbb{C}^M$ .

### A. Channel models

Each of the previously mentioned channels is modeled in accordance to [11], which accurately captures the spatial sparsity that characterizes mmWave channels. Each channel consists of contributions from  $C_i$  scattering clusters, i.e.,

$$\mathbf{b}_r = \underbrace{\sqrt{\beta_{0,r}^2} \mathbf{a}_M(\boldsymbol{\omega}_{0,r})}_{\bar{\mathbf{b}}_r} + \sqrt{\frac{1}{C_1}} \sum_{n=1}^{C_1} \alpha_{n,r} \mathbf{a}_M(\boldsymbol{\omega}_{n,r}), \quad (1)$$

$$\mathbf{g}_T = \underbrace{\sqrt{\beta_{0,T}^2} \mathbf{a}_N(\boldsymbol{\omega}_{0,T})}_{\bar{\mathbf{g}}_T} + \sqrt{\frac{1}{C_2}} \sum_{n=1}^{C_2} \alpha_{n,T} \mathbf{a}_N(\boldsymbol{\omega}_{n,T}), \quad (2)$$

$$\mathbf{g}_{k,t} = \sqrt{\frac{1}{C_3}} \sum_{n=1}^{C_3} \alpha_{n,k,t} \mathbf{a}_M(\boldsymbol{\omega}_{n,k,t}), \quad (3)$$

$$\mathbf{H}_t = \underbrace{\sqrt{\beta_{0,t,T}^2} \mathbf{a}_N(\boldsymbol{\omega}_{0,t,T}^{\text{RIS}}) \mathbf{a}_M^\top(\boldsymbol{\omega}_{0,t,T}^{\text{AP}})}_{\bar{\mathbf{H}}_t} + \sqrt{\frac{1}{C_4}} \sum_{n=1}^{C_4} \alpha_{n,t,T} \mathbf{a}_N(\boldsymbol{\omega}_{n,t,T}^{\text{RIS}}) \mathbf{a}_M^\top(\boldsymbol{\omega}_{n,t,T}^{\text{AP}}), \quad (4)$$

where the overline superscript indicates the LoS paths and the other terms correspond to the NLoS parts. The  $\beta_{0,r}^2$ ,  $\beta_{0,T}^2$ , and  $\beta_{0,t,T}^2$  are the corresponding LoS channel gains. We now remove the additional subscripts after  $n$  as the following consideration applies regardless of the additional subscripts. Here,  $\alpha_n$  is the complex channel gain of the  $n$ -th cluster. We assume each cluster scatters a sufficient number of rays such that  $\alpha_n \sim \mathcal{CN}(0, \beta_n^2)$  and the fading is mutually independent. The coefficients  $\beta_n^2$  represent the path loss associated with the respective clusters. The geometry of the  $n$ -th cluster is described by  $\boldsymbol{\omega}_n = [\psi_n, \phi_n]$ , where  $\psi_n$  is the azimuth angle and  $\phi_n$  is the elevation angle. Each AP is equipped with a uniform planar square array with a half-wavelength vertical and horizontal inter-element spacing such that the entries of  $M$ -dimensional steering vector are defined as

$$[\mathbf{a}_M(\boldsymbol{\omega}_n)]_{m_h, m_v} = e^{-j\pi(m_h \sin(\psi_n) \cos(\phi_n) + m_v \sin(\phi_n))} \quad (5)$$

for  $m_h, m_v = 0, \dots, \sqrt{M} - 1$ . We assume that perfect CSI for  $\{\mathbf{g}_{k,t}\}_{\forall k,t}$  is available at the APs, as this is easily obtainable through well-known estimation techniques. As for the sensing channels, the transmit APs only know the position of the RIS and the target and, thus, the corresponding LoS channels.

### B. Communication observation model

We assume that the APs are equipped with fully digital beamforming hardware:  $\mathbf{f}_{t,l}$  is the precoding vector for stream  $l$  and AP  $t$ , and  $\mathbf{F}_t = [\mathbf{f}_{1,t}, \dots, \mathbf{f}_{L,t}] \in \mathbb{C}^{M \times L}$ , where  $L = K + 1$ . Here, we allocate one beam to each UE and an additional one, denoted by the index  $L$ , for sensing purposes, bringing the total number of digital beams to  $L = K + 1$ . This choice is motivated by the fact that the UEs and target typically are at very different positions, and catering solely to the communication UEs might drastically reduce the system's sensing performance.

The received downlink signal at UE  $k$  during timeslot  $\tau$  is defined as

$$y_k[\tau] = \sum_{t \in \mathcal{T}} \mathbf{g}_{k,t}^H \mathbf{s}_t[\tau] + w_k[\tau] = \sum_{t \in \mathcal{T}} \underbrace{\left( \sqrt{\rho_k} \mathbf{g}_{k,t}^H \mathbf{f}_{k,t} x_k[\tau] \right)}_{\text{desired signal}} \quad (6)$$

$$+ \underbrace{\sum_{k' \in \mathcal{K} \setminus \{k\}} \sqrt{\rho_{k'}} \mathbf{g}_{k,t}^H \mathbf{f}_{k',t} x_{k'}[\tau]}_{\text{multi-user interf. (MUI)}} + \underbrace{\sqrt{\rho_L} \mathbf{g}_{k,t}^H \mathbf{f}_{L,t} x_L[\tau]}_{\text{sensing interf.}} + w_k[\tau],$$

with  $\mathbf{s}_t[\tau] = \mathbf{F}_t \mathbf{X}[\tau] \boldsymbol{\rho}$ , where the matrix  $\mathbf{X}[\tau] = \text{diag}(x_1[\tau], \dots, x_L[\tau])$  is a diagonal matrix containing the common downlink communication symbols transmitted during timeslot  $\tau$ , where each of them is assumed to be of unit power. Lastly, the vector  $\boldsymbol{\rho} = [\sqrt{\rho_1}, \dots, \sqrt{\rho_L}]^\top$  contains the square root of the power allocated to each beam. Finally,  $w_k[\tau] \sim \mathcal{CN}(0, \sigma_k^2)$ .

In line with the centralized operation of cell-free massive MIMO, the communication precoding vectors are based on the transmit APs CSI [3] while the sensing precoder is based on the assumed LoS structure of the sensing channels and the known target location. To this end, we define  $\mathbf{g}_k = [\mathbf{g}_{k,1}^\top, \dots, \mathbf{g}_{k,T}^\top]^\top \in \mathbb{C}^{MT}$  and  $\mathbf{f}_k = [\mathbf{f}_{k,1}^\top, \dots, \mathbf{f}_{k,T}^\top]^\top \in \mathbb{C}^{MT}$ . The communication precoding vectors for each UE are chosen using RZF as

$$\mathbf{f}_k = \frac{(\sum_{i \in \mathcal{K}} \mathbf{g}_i \mathbf{g}_i^H + \lambda \mathbf{I}_{MT})^{-1} \mathbf{g}_k}{\left\| (\sum_{i \in \mathcal{K}} \mathbf{g}_i \mathbf{g}_i^H + \lambda \mathbf{I}_{MT})^{-1} \mathbf{g}_k \right\|}, \quad k = 1, \dots, K, \quad (7)$$

where  $\lambda$  is a regularization parameter and this parameter allows the system to implement a trade-off between interference and noise suppression. For the sensing stream, let us define the matrix  $\mathbf{G} = [\mathbf{g}_1, \dots, \mathbf{g}_K] \in \mathbb{C}^{MT \times K}$  with all the UE channels. Then the sensing stream precoder is defined as

$$\mathbf{f}_{L,t} = \frac{(\mathbf{I}_{MT} - \mathbf{G} (\mathbf{G}^H \mathbf{G})^\dagger \mathbf{G}^H) \bar{\mathbf{h}}_T}{\left\| (\mathbf{I}_{MT} - \mathbf{G} (\mathbf{G}^H \mathbf{G})^\dagger \mathbf{G}^H) \bar{\mathbf{h}}_T \right\|}, \quad (8)$$

where  $\bar{\mathbf{h}}_T = [\bar{\mathbf{h}}_{T,1}^\top, \dots, \bar{\mathbf{h}}_{T,T}^\top]^\top$  and  $\bar{\mathbf{h}}_{T,t} = \bar{\mathbf{H}}_t^\top \boldsymbol{\Theta} \bar{\mathbf{g}}_T$  with  $\boldsymbol{\Theta} = \text{diag}(\boldsymbol{\theta})$ . We have projected  $\bar{\mathbf{h}}_T$  onto the null space of the communication UEs' channels to null the interference caused to the UEs. The communication performance is represented by the UEs' spectral efficiency (SE), defined as  $\text{SE}_k = \log_2(1 + \text{SINR}_k)$ : under the assumption of perfect CSI on the UEs channels, the SINR is defined as

$$\text{SINR}_k = \frac{|\mathbf{g}_k^H \mathbf{f}_k \sqrt{\rho_k}|^2}{\sum_{k' \in \mathcal{K}/k} |\mathbf{g}_k^H \mathbf{f}_{k'} \sqrt{\rho_{k'}}|^2 + |\mathbf{g}_k^H \mathbf{f}_L \sqrt{\rho_L}|^2 + \sigma_k^2}. \quad (9)$$

### C. Sensing observation model

The two-way sensing channel between transmit AP  $t$  and receive AP  $r$  is defined as

$$\mathbf{E}_{t,r} = \mathbf{b}_r \mathbf{h}_{t,r}^H \triangleq \mathbf{b}_r (\mathbf{H}_t^H \boldsymbol{\Theta} \mathbf{g}_T)^H. \quad (10)$$

The sensing observation of AP  $r$  at timeslot  $\tau$  is

$$\mathbf{y}_r[\tau] = \sum_{t \in \mathcal{T}} c_{t,r} \mathbf{E}_{t,r} \mathbf{s}_t[\tau] + \mathbf{z}_r[\tau] + \mathbf{n}_r[\tau], \quad (11)$$

where  $c_{t,r}$  is the radar cross section (RCS) associated with the sensing path between transmit AP  $t$  and receive AP  $r$ . We adopt the Swerling-I model, meaning that the RCS assumes only one value during the transmission and  $c_{t,r} \sim \mathcal{CN}(0, \delta_{t,r}^2)$ . We assume that  $\{\delta_{t,r}^2\}_{\forall t,r}$  are known and that RCSs belonging to different transmit-receiving pairs are statistically uncorrelated, that is

$$\mathbb{E} \{ c_{a,r} c_{a',r'}^* \} = \begin{cases} \delta_{a,r}^2, & \text{if } a = a', r = r', \\ 0, & \text{otherwise.} \end{cases} \quad (12)$$

In (11),  $\mathbf{n}_r[\tau]$  is the receiver noise of AP  $r$ , assumed to have independent  $\mathcal{CN}(0, \sigma^2)$  entries. The vector  $\mathbf{z}_r[\tau]$  represents the target's clutter as observed from AP  $r$ . The clutter vector is modeled as  $\mathbf{z}_r[\tau] \sim \mathcal{CN}(\mathbf{0}, \delta_z^2 \mathbf{R}_r)$ , where  $\delta_z^2$  is the power of the clutter cross section, which also includes the path loss effects, thus defining the CNR as  $\text{CNR} = \delta_z^2 / \sigma^2$ . The normalized clutter covariance matrix with trace being equal to  $M$  is denoted by  $\mathbf{R}_r$ . This matrix is unknown, but its eigenspace is assumed to be known later in the detector design. For the sake of mathematical tractability, we assume that the clutter observations belonging to different APs and/or different timeslots are statistically uncorrelated. Under the LoS assumption for the channels involved in sensing, the target's SCNR is defined as

$$\overline{\text{SCNR}} = \frac{\sum_{\tau=1}^U \sum_{r \in \mathcal{R}} \sum_{a \in \mathcal{T}} \delta_{a,r}^2 \|\bar{\mathbf{E}}_{a,r} \mathbf{s}_a[\tau]\|^2}{RUM (\sigma^2 + \delta_z^2)}. \quad (13)$$

## III. SENSING PERFORMANCE OPTIMIZATION

The system aims at jointly maximizing the sensing SCNR (13) while guaranteeing a minimum SINR to all the communication UEs. The optimization problem is stated as follows:

$$\underset{\boldsymbol{\theta}, \boldsymbol{\rho}}{\text{maximize}} \quad \overline{\text{SCNR}} \quad (14a)$$

$$\text{subject to} \quad \text{SINR}_k \geq \gamma_k, \quad \forall k \in \mathcal{K}, \quad (14b)$$

$$\sum_{l=1}^L \|\mathbf{f}_{l,t}\|^2 \rho_l \leq P_t, \quad \forall t \in \mathcal{T}, \quad (14c)$$

$$|\theta_n| = 1, \quad n = 1, \dots, N, \quad (14d)$$

where  $\gamma_k$  is the SINR threshold of UE  $k$  and  $P_t$  is the available transmit power of the  $t$ -th AP. This problem is non-convex, mainly due to the coupling between the optimization variables and the non-convex unitary modulus constraints. In this section, we will devise an AO algorithm, which switches between optimizing the power allocation policy and the RIS phase shifts until convergence is achieved.

### A. Power allocation optimization

In this subsection, we introduce the first subproblem of the AO algorithm, where we optimize the power allocation for a fixed RIS configuration. We first reformulate (13) as

$$\overline{\text{SCNR}} = \boldsymbol{\rho}^\top \Re(\mathbf{A}) \boldsymbol{\rho}, \quad (15)$$

where

$$\mathbf{A} = \frac{\sum_{\tau=1}^U \sum_{r \in \mathcal{R}} \sum_{a \in \mathcal{T}} \delta_{a,r}^2 \mathbf{X}^H[\tau] \mathbf{F}_a^H \bar{\mathbf{E}}_{a,r}^H \bar{\mathbf{E}}_{a,r} \mathbf{F}_a \mathbf{X}[\tau]}{RUM(\sigma^2 + \delta_z^2)}. \quad (16)$$

The set of constraints (14b) can be reformulated as a second order cone (SOC) constraints in terms of  $\boldsymbol{\rho}$  as

$$\left\| \left[ \begin{array}{c|c|c|c|c} \mathbf{g}_k^H \mathbf{f}_1 | \sqrt{\rho_1} & \dots & \underbrace{0}_k & \dots & \mathbf{g}_k^H \mathbf{f}_L | \sqrt{\rho_L} \quad \sigma_k \end{array} \right] \right\| \leq \frac{|\mathbf{g}_k^H \mathbf{f}_k| \sqrt{\rho_k}}{\sqrt{\gamma_k}}. \quad (17)$$

The power constraint in (14c) can also be rewritten as a SOC as

$$\|\text{diag}(\|\mathbf{f}_{1,t}\|, \dots, \|\mathbf{f}_{L,t}\|)\boldsymbol{\rho}\| \leq \sqrt{P_t}. \quad (18)$$

The first subproblem of the AO SCNR-maximizing algorithm is defined as

$$\underset{\boldsymbol{\rho}}{\text{maximize}} \quad \boldsymbol{\rho}^\top \Re(\mathbf{A})\boldsymbol{\rho} \quad (19a)$$

$$\text{subject to (17), (18)}. \quad (19b)$$

This problem can be solved using the convex-concave procedure outlined in [3].

### B. RIS phase-shift optimization

We now move on to the second part of the AO, where we optimize  $\boldsymbol{\theta}$  when the power variables are fixed. The SCNR can be reformulated as

$$\overline{\text{SNR}}_T = \boldsymbol{\theta}^H \mathbf{Q} \boldsymbol{\theta}, \quad (20)$$

where

$$\mathbf{Q} = \frac{1}{RUM(\sigma^2 + \delta_z^2)} \sum_{\tau=1}^U \sum_{r \in \mathcal{R}} \sum_{a \in \mathcal{T}} \left( \delta_{a,r}^2 \bar{\mathbf{g}}_T^H \bar{\mathbf{b}}_r^H \bar{\mathbf{b}}_r \bar{\mathbf{g}}_T \right)^\top \odot \left( \bar{\mathbf{H}}_a \mathbf{s}_a[\tau] \mathbf{s}_a^H[\tau] \bar{\mathbf{H}}_a^H \right). \quad (21)$$

We have used  $\text{Tr}(\mathbf{A}\mathbf{X}\mathbf{B}\mathbf{X}^H) = \text{vec}^H(\mathbf{X})(\mathbf{B}^\top \otimes \mathbf{A})\text{vec}(\mathbf{X})$  and the following lemma.

**Lemma 1.** Let  $\mathbf{x} \in \mathbb{C}^N$  and  $\mathbf{X} = \text{diag}(\mathbf{x})$ . For any  $\mathbf{A} \in \mathbb{C}^{N \times N}$  and  $\mathbf{B} \in \mathbb{C}^{N \times N}$ , it holds that

$$\text{vec}^H(\mathbf{X})(\mathbf{A} \otimes \mathbf{B})\text{vec}(\mathbf{X}) = \mathbf{x}^H(\mathbf{A} \odot \mathbf{B})\mathbf{x}. \quad (22)$$

**Proof:** Let  $\text{vec}(\mathbf{X}) = \sum_{n=1}^N x_n \mathbf{e}_n \otimes \mathbf{e}_n$ , where  $\mathbf{e}_n$  is the  $n$ -th column of  $\mathbf{I}_N$ . Then, the right-hand side of (22) can be written as  $\left( \sum_{n=1}^N x_n \mathbf{e}_n \otimes \mathbf{e}_n \right)^H (\mathbf{A} \otimes \mathbf{B}) \left( \sum_{m=1}^N x_m \mathbf{e}_m \otimes \mathbf{e}_m \right) \stackrel{(a)}{=} \sum_{n=1}^N \sum_{m=1}^N x_n x_m^H (\mathbf{e}_n^H \mathbf{A} \mathbf{e}_m) (\mathbf{e}_n^H \mathbf{B} \mathbf{e}_m) = \sum_{n=1}^N \sum_{m=1}^N x_n x_m^H [\mathbf{A}]_{n,m} [\mathbf{B}]_{n,m} = \mathbf{x}^H(\mathbf{A} \odot \mathbf{B})\mathbf{x}$ , where in (a) we used mixed-product property of the Kronecker product. ■

The RIS phase-shift optimization problem under consideration is still non-convex. We are trying to maximize a quadratic form of  $\boldsymbol{\theta}$ . We then employ the minorization-maximization (MM) algorithm to maximize a convex lower bound on (20)

[12]. More specifically, a convex local lower bound can be found by applying the successive convex approximation [13] around the local point  $\boldsymbol{\theta}^{(s)}$  at iteration  $s$ . The objective function can be lower bounded by

$$\boldsymbol{\theta}^H \mathbf{Q} \boldsymbol{\theta} \geq 2\Re \left( \boldsymbol{\theta}^{(s)H} \mathbf{Q}^{(+)} \boldsymbol{\theta} \right) + \boldsymbol{\theta}^H \mathbf{Q}^{(-)} \boldsymbol{\theta} - \boldsymbol{\theta}^{(s)H} \mathbf{Q}^{(+)} \boldsymbol{\theta}^{(s)}, \quad (23)$$

where  $\mathbf{Q}^{(+)}$  and  $\mathbf{Q}^{(-)}$  represents the positive and negative semidefinite parts of  $\mathbf{Q}$ . We can now define the second subproblem of the AO optimization as

$$\underset{\boldsymbol{\theta}, \alpha \geq 0}{\text{maximize}} \quad \alpha \quad (24a)$$

$$\text{subject to } \alpha \leq 2\Re \left( \boldsymbol{\theta}^{(s)H} \mathbf{Q}^{(+)} \boldsymbol{\theta} \right) + \boldsymbol{\theta}^H \mathbf{Q}^{(-)} \boldsymbol{\theta} - \boldsymbol{\theta}^{(s)H} \mathbf{Q}^{(+)} \boldsymbol{\theta}^{(s)}, \quad (24b)$$

$$|\theta_n| \leq 1, \quad n = 1, \dots, N, \quad (24c)$$

where  $\alpha$  is an auxiliary variable. Note that we have relaxed the unit modulus constraint, as it is observed that the solution satisfies this constraint with equality anyway. This is a convex problem and can be solved at each iteration until convergence is achieved. The steps of the AO algorithm are outlined in Algorithm 1.

---

### Algorithm 1: SCNR maximizing AO algorithm

---

- 1: **Initialize:** Generate  $\boldsymbol{\theta}^{(0)}$  randomly,  $v \leftarrow 0$
  - 2: **repeat**
  - 3:   Compute the precoding codebooks with  $\boldsymbol{\theta} = \boldsymbol{\theta}^{(v)}$
  - 4:   Obtain  $\boldsymbol{\rho}^{(v+1)}$  by solving (19)
  - 5:   Obtain  $\boldsymbol{\theta}^{(v+1)}$  by solving (24) iteratively
  - 6:    $v \leftarrow v + 1$
  - 7: **until** Convergence
  - 8: **Output:**  $\boldsymbol{\theta}^{\text{opt}}, \boldsymbol{\rho}^{\text{opt}}$
- 

## IV. GLRT DETECTOR

One of the main metrics used to assess the sensing performance is the probability of correct detection, implemented through a GLRT by extending the detector in [9] to a cell-free massive MIMO system based on the optimization procedure developed in the previous section. We operate under the assumption that the transmit signals are known by the receiving APs, thanks to the cell-free architecture. We define the vector containing the combined sensing observation of all receiving APs during timeslot  $\tau$  as

$$\mathbf{y}[\tau] = [\mathbf{y}_1^\top[\tau], \dots, \mathbf{y}_R^\top[\tau]]^\top = \mathbf{V}[\tau]\mathbf{c} + \mathbf{U}\mathbf{w}[\tau] + \mathbf{n}[\tau], \quad (25)$$

$$\mathbf{V}[\tau] = \text{blkdiag}(\mathbf{V}_1[\tau], \dots, \mathbf{V}_R[\tau]) \in \mathbb{C}^{MR \times TR}, \quad (26)$$

$$\mathbf{V}_r[\tau] = [\mathbf{E}_{1,r} \mathbf{s}_1[\tau], \dots, \mathbf{E}_{T,r} \mathbf{s}_T[\tau]] \in \mathbb{C}^{M \times T}, \quad (27)$$

$$\mathbf{n}[\tau] = [\mathbf{n}_1^\top[\tau], \dots, \mathbf{n}_R^\top[\tau]]^\top, \quad \mathbf{c} = [c_{1,1}, \dots, c_{T,R}]^\top, \quad (28)$$

$$\mathbf{U} = \text{blkdiag}(\mathbf{U}_1, \dots, \mathbf{U}_R), \quad \mathbf{w}[\tau] = [\mathbf{w}_1^\top[\tau], \dots, \mathbf{w}_R^\top[\tau]]^\top. \quad (29)$$

The clutter observed by AP  $r$  is assumed to exist in a low-rank subspace [14] spanned by the columns of the semi-unitary

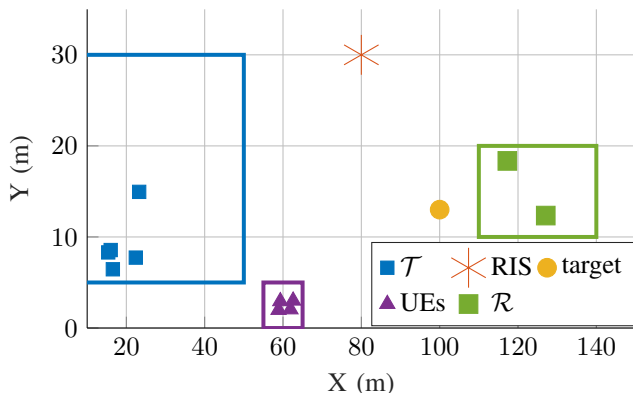


Fig. 2: 2D locations in the simulated scenario.

matrix  $\mathbf{U}_r \in \mathbb{C}^{M \times i}$ , with  $i$  being the subspace dimension, obtained through the eigendecomposition of  $\delta_z^2 \mathbf{R}_r$ . AP  $r$ 's clutter is then expressed as  $\mathbf{U}_r \mathbf{w}_r[\tau]$ , where the distribution of  $\mathbf{w}_r[\tau]$  is unknown. The previous observations are generated using the true channels; however, the system does not have perfect CSI on the sensing channels and thus assumes a LoS structure. Therefore, the binary hypotheses being tested are

$$\mathcal{H}_0 : \mathbf{y}[\tau] = \bar{\mathbf{V}}[\tau] \mathbf{c} + \mathbf{U} \mathbf{w}[\tau] + \mathbf{n}[\tau], \quad \tau = 1, \dots, U, \quad (30)$$

$$\mathcal{H}_1 : \mathbf{y}[\tau] = \mathbf{U} \mathbf{w}[\tau] + \mathbf{n}[\tau], \quad \tau = 1, \dots, U, \quad (31)$$

where  $\bar{\mathbf{V}}$  is computed as  $\mathbf{V}$  by using  $\bar{\mathbf{E}}_{t,r}$ . The adoption of a GLRT method is motivated by the unknown distribution of  $\mathbf{w}[\tau]$ , however we know that  $\mathbf{y}_{\mathcal{H}_0}[\tau] - \mathbf{U} \mathbf{w}[\tau] \sim \mathcal{CN}(0, \sigma^2 \mathbf{I}_{MR})$  and  $\mathbf{y}_{\mathcal{H}_1}[\tau] - \mathbf{U} \mathbf{w}[\tau] \sim \mathcal{CN}(0, \mathbf{R}[\tau] + \sigma^2 \mathbf{I}_{MR})$ , where  $\mathbf{R}[\tau] = \mathbb{E} \left\{ \bar{\mathbf{V}}[\tau] \mathbf{c} \mathbf{c}^H \bar{\mathbf{V}}^H[\tau] \right\} = \bar{\mathbf{V}}[\tau] \text{diag}(\delta_{1,1}^2, \dots, \delta_{T,R}^2) \bar{\mathbf{V}}[\tau]^H$ . The GLRT test is then defined as

$$\frac{\prod_{\tau=1}^U \max_{\mathbf{w}[\tau]} f_{\mathbf{y}[\tau]|\mathbf{w}[\tau], \mathcal{H}_1}(\mathbf{y}[\tau]|\mathbf{w}[\tau], \mathcal{H}_1)}{\prod_{\tau=1}^U \max_{\mathbf{w}[\tau]} f_{\mathbf{y}[\tau]|\mathbf{w}[\tau], \mathcal{H}_0}(\mathbf{y}[\tau]|\mathbf{w}[\tau], \mathcal{H}_0)} \stackrel{\mathcal{H}_0}{\leq} \lambda_d, \quad (32)$$

where  $f_{\mathbf{y}[\tau]|\mathbf{w}[\tau], \mathcal{H}}$  denote the probability density function. Following the derivation in [9], the GLRT test can be rewritten as

$$\sum_{\tau=1}^U \mathbf{y}^H[\tau] \mathbf{T}[\tau] \mathbf{y}[\tau] \stackrel{\mathcal{H}_0}{\leq} \underbrace{\ln(\lambda_d) - \ln(\varsigma)}_{\tilde{\lambda}_d} \quad (33)$$

$$\mathbf{T}[\tau] = \mathbf{\Xi}[\tau] \mathbf{U} \left( \mathbf{U}^H \mathbf{\Xi}[\tau] \mathbf{U} \right)^{-1} \mathbf{U}^H \mathbf{\Xi}[\tau] + \sigma^{-2} (\mathbf{I}_{MR} - \mathbf{U} \mathbf{U}^H) - \mathbf{\Xi}[\tau] \quad (34)$$

$$\mathbf{\Xi}[\tau] = (\mathbf{R}[\tau] + \sigma^2 \mathbf{I}_{MR})^{-1} \quad (35)$$

where  $\varsigma = \det(\sigma^2 \mathbf{I}_{MR})^U / \prod_{\tau=1}^U \det(\mathbf{R}[\tau] + \sigma^2 \mathbf{I}_{MR})$ .  $\tilde{\lambda}_d$  is a revised threshold whose value should be chosen according to the desired false alarm probability, and it can be computed through Monte Carlo trials.

## V. NUMERICAL RESULTS

In this section, the numerical simulation results are provided. A two-dimensional view of the simulated scenario is provided in Fig. 2. The locations of the transmit APs in  $\mathcal{T}$ ,

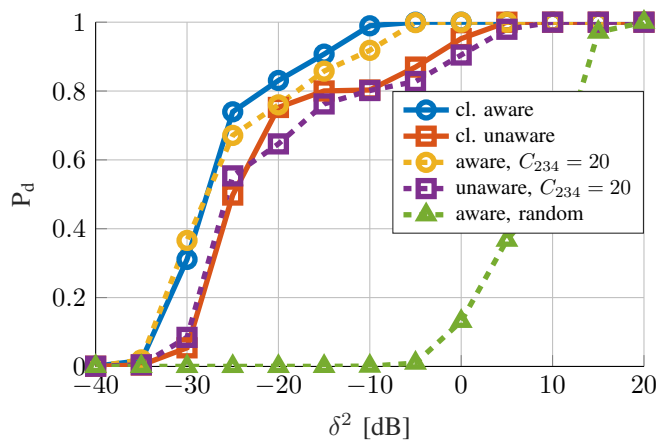


Fig. 3: Probability of detection with respect to the RCS power with a CNR of 20 dB.

the receiving ones in  $\mathcal{R}$ , and the UEs are randomly generated within the respective bounding boxes, and their  $z$  coordinates are equal to 10 m, 10 m, and 1 m respectively. The RIS and target position are assumed to be fixed and their  $z$  coordinates are equal to 15 m and 3 m. The power budget for each transmit AP is 2 dBW, with a bandwidth of  $B = 1$  MHz, the noise power is equal to  $-204 + 10 \log_{10}(B)$  dBW. The channel's path loss follows the 3GPP urban microcell model defined in [15]. The clutter is modeled according to the local scattering model in [16] with six clusters centered around the  $20^\circ$  and  $10^\circ$  neighborhoods of the  $\omega_{0,r}$ . We have  $T = 5$  transmit APs and  $R = 2$  receiving APs, each equipped with  $M = 36$  antennas and serving  $K = 5$  UEs. We want to guarantee an SINR of  $\gamma_k = 3$  dB to all UEs. Unless otherwise specified, the RIS is equipped with  $N = 64$  elements,  $C_1 = C_2 = C_3 = C_4 = 2$ , and the angles are uniformly distributed within an angle spread of  $\sigma_{\psi_n} = 10^\circ$  in azimuth and  $\sigma_{\phi_n} = 10^\circ$  in elevation around the LoS angles between transmitter and receiver, denoted by  $\psi_0$  ( $\phi_0$ ). The results shown hereafter are averaged over 10 random realizations of the AP positions and UE positions. For each of these realizations, the probability of detection is computed over  $U = 5$  timeslots and  $1000U$  noise and clutter realizations. The false alarm probability is set to  $10^{-4}$ .

### A. Clutter awareness and cluster number's impact

We first analyze the impact of the clutter awareness of the receiving APs on the detection probability and how much the LoS assumed structure of the channels affects the system's detection performances when there are many clusters concentrated within a small angular region. Fig. 3 shows this probability of detection vs. the RCS power, where we assumed that  $\delta_{1,1}^2 = \dots = \delta_{T,R}^2 = \delta^2$  for a CNR of 20 dB. We can see that a clutter-aware system outperforms a clutter-unaware one. On the other hand, when  $C_2 = C_3 = C_4 = 20$ , here denoted by  $C_{234}$ , the LoS assumption does not hold as much, thus generating a performance decrease. Our optimized model greatly outperforms a benchmark approach, consisting of a random RIS phase-shift matrix and an equal power allocation

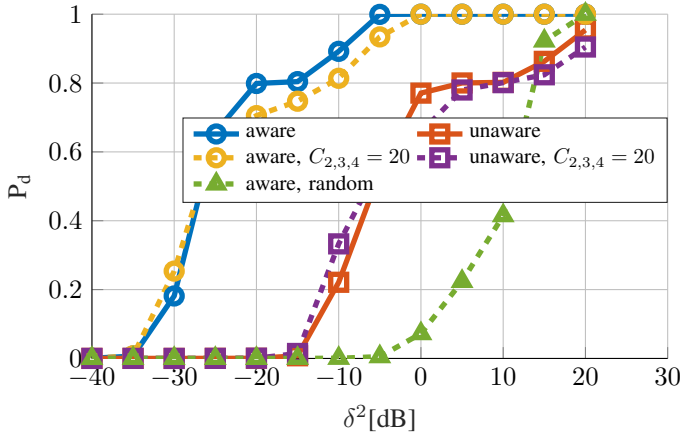


Fig. 4: Probability of detection with respect to the RCS power with a CNR of 40 dB.

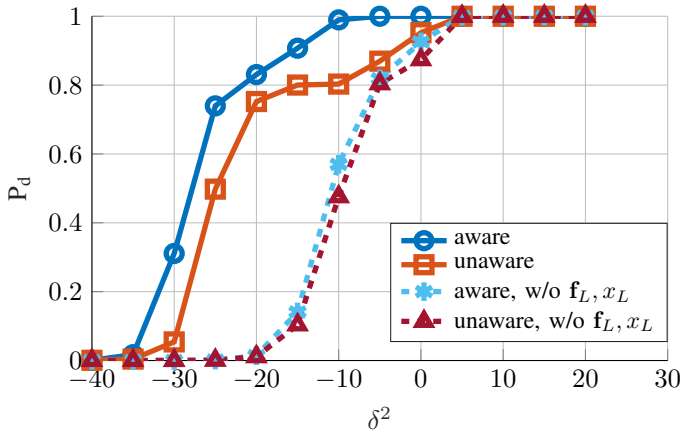


Fig. 5: Impact of a dedicated sensing stream onto the probability of detection with a CNR of 20 dB.

between the beams. Fig. 4 shows what happens when the CNR rises to 40 dB. We see that clutter awareness rises in importance, widening the gap between the clutter-aware and unaware detectors.

### B. Do we need dedicated sensing symbols?

Given the sparse nature of the mmWave channels, one might question whether or not a dedicated sensing stream is necessary and to what extent the system benefits from it. To gain more insight into this, we have analyzed a system without sensing-dedicated precoding. Fig. 5 compares the detection performance of systems with and without dedicated sensing precoding, both in the presence and in the absence of clutter awareness. We can immediately see that removing the sensing streams implies a performance degradation. Interestingly, the system without sensing dedicated precoding seems to suffer less from the lack of clutter awareness at a low RCS value.

## VI. CONCLUSIONS

We have investigated a cell-free massive MIMO ISAC network jointly serving multiple communication UEs while detecting a potential target through an RIS in a multi-static

fashion. The system wants to maximize its sensing performance while preserving a minimum SINR for the communication UEs. To this end, we optimize the power allocation of a precoding codebook jointly with the RIS phase-shift matrix and we derive the sufficient statistics for the target detector. Numerical results show that clutter awareness at the receiving APs plays a crucial role in the system's detection performance and that including a dedicated sensing stream benefits the system. We see that the mmWave channel structure makes the allow the system to assume LoS channels and still achieve good performances when the channel is composed of a high number of clusters concentrated in a small angular range.

## REFERENCES

- [1] Ö. T. Demir, E. Björnson, and L. Sanguinetti, "Foundations of user-centric cell-free massive MIMO," *Foundations and Trends® in Signal Processing*, vol. 14, no. 3-4, pp. 162–472, 2021.
- [2] H. Q. Ngo, G. Interdonato, E. G. Larsson, G. Caire, and J. G. Andrews, "Ultradense cell-free massive MIMO for 6G: Technical overview and open questions," *Proceedings of the IEEE*, 2024.
- [3] Z. Behdad, Ö. T. Demir, K. W. Sung, E. Björnson, and C. Cavdar, "Multi-static target detection and power allocation for integrated sensing and communication in cell-free massive MIMO," *IEEE Transactions on Wireless Communications*, vol. 23, no. 9, pp. 11 580–11 596, 2024.
- [4] U. Demirhan and A. Alkhateeb, "Cell-free ISAC MIMO systems: Joint sensing and communication beamforming," *IEEE Transactions on Communications*, 2024.
- [5] S. Lu, F. Liu, Y. Li, K. Zhang, H. Huang, J. Zou, X. Li, Y. Dong, F. Dong, J. Zhu *et al.*, "Integrated sensing and communications: Recent advances and ten open challenges," *IEEE Internet of Things Journal*, 2024.
- [6] G. C. Alexandropoulos, N. Shlezinger, and P. Del Hougne, "Reconfigurable intelligent surfaces for rich scattering wireless communications: Recent experiments, challenges, and opportunities," *IEEE Communications Magazine*, vol. 59, no. 6, pp. 28–34, 2021.
- [7] K. Chen, C. Qi, O. A. Dobre, and G. Y. Li, "Simultaneous beam training and target sensing in ISAC systems with RIS," *IEEE Transactions on Wireless Communications*, 2023.
- [8] R. Liu, M. Li, and A. L. Swindlehurst, "Joint beamforming and reflection design for RIS-assisted ISAC systems," in *2022 30th European Signal Processing Conference (EUSIPCO)*. IEEE, 2022, pp. 997–1001.
- [9] Ö. T. Demir and E. Björnson, "RIS-assisted ISAC: Precoding and phase-shift optimization for mono-static target detection," *arXiv preprint arXiv:2410.06855*, 2024.
- [10] C. He, Y. Ma, S. Wei, and J. Zhang, "Research on adaptive self-interference cancellation and sensing methods in ISAC system," in *2024 International Wireless Communications and Mobile Computing (IWCMC)*. IEEE, 2024, pp. 921–926.
- [11] J. Zhang, X. Yu, and K. B. Letaief, "Hybrid beamforming for 5G and beyond millimeter-wave systems: A holistic view," *IEEE Open Journal of the Communications Society*, vol. 1, pp. 77–91, 2019.
- [12] Z.-M. Jiang, M. Rihan, P. Zhang, L. Huang, Q. Deng, J. Zhang, and E. M. Mohamed, "Intelligent reflecting surface aided dual-function radar and communication system," *IEEE Systems Journal*, vol. 16, no. 1, pp. 475–486, 2021.
- [13] O. Mehanna, K. Huang, B. Gopalakrishnan, A. Konar, and N. D. Sidiropoulos, "Feasible point pursuit and successive approximation of non-convex QCQPs," *IEEE Signal Processing Letters*, vol. 22, no. 7, pp. 804–808, 2014.
- [14] A. Breloy, G. Ginolhac, F. Pascal, and P. Forster, "Clutter subspace estimation in low rank heterogeneous noise context," *IEEE Transactions on Signal Processing*, vol. 63, no. 9, pp. 2173–2182, 2015.
- [15] 3GPP, "Technical specification group radio access network; channel model for frequency spectrum above 6 GHz (release 14)," 2016.
- [16] Ö. T. Demir, E. Björnson, and L. Sanguinetti, "Channel modeling and channel estimation for holographic massive MIMO with planar arrays," *IEEE Wireless Communications Letters*, vol. 11, no. 5, pp. 997–1001, 2022.